Annals of Physics 471 (2024) 169837

Contents lists available at ScienceDirect

Annals of Physics

journal homepage: www.elsevier.com/locate/aop

Topological flat band with higher winding number in a superradiance lattice

Shuai Li [a,1], Rui Tian [a,1], Min Liu [a], Maksims Arzamasovs [a], Liangchao Chen [b], Bo Liu [a,*]

[a] Ministry of Education Key Laboratory for Nonequilibrium Synthesis and Modulation of Condensed Matter, Shaanxi Province Key Laboratory of Quantum Information and Quantum Optoelectronic Devices, School of Physics, Xi'an Jiaotong University, Xi'an 710049, China

[b] State Key Laboratory of Quantum Optics and Quantum Optics Devices, Institute of Opto-electronics, Shanxi University, Taiyuan, Shanxi 030006, People's Republic of China

ARTICLE INFO

Keywords:
Flat band
Higher winding number
Quantum simulation
Topological states of matter

ABSTRACT

A five-level M-type scheme in atomic ensembles is proposed to generate a one-dimensional bipartite superradiance lattice in momentum space. By taking advantage of this tunable atomic system, we show that various types of Su-Schrieffer-Heeger (SSH) model, including the standard SSH and extended SSH model, can be realized. Interestingly, it is shown that through changing the Rabi frequencies and detunings in our proposed scheme, there is a topological phase transition from topological trivial regime with winding number being 0 to topological non-trivial regime with winding number being 2. Furthermore, a robust flat band with higher winding number (being 2) can be achieved in the above topological non-trivial regime, where the superradiance spectra can be utilized as a tool for experimental detection. Our proposal would provide a promising approach to explore new physics, such as fractional topological phases, in the flat bands with higher topological number.

1. Introduction

There has been a surge of interest in flat band physics [1], where one or more dispersionless bands exist throughout the Brillouin zone. Many theoretical proposals for searching flat band systems have been made [2–10] and its captivation has become exceptionally pronounced following the experimental realization in twisted bilayer graphene [11–14]. Due to the macroscopic level degeneracy in flat bands, lots of interesting physical phenomena, such as ferromagnetism [3,7,9,15,16], Wigner crystals [17] and superconductivity [18,19], can be induced. In particular, isolated flat bands with non-trivial topological properties have also attracted much attention, since fractional topological phases, such as fractional quantum Hall and fractional Chern insulator states [20–28], can be simulated without Landau levels. More interestingly, the flat bands with higher topological number (e.g., higher Chern number) can host qualitatively new phases of matter with no analogue in the flat band being similar to the continuum Landau level [29–31]. New types of intriguing fractional Chern insulator states, for fermions at $\nu = 1/2N + 1$ and for bosons at $\nu = 1/N + 1$, are unveiled [31]. Distinguished from the cases in 2D, 1D topological nontrivial flat bands can unusually lead to new physical phenomena, for instance, a charge density wave with a nontrivial Berry phase, which is not a 1D analog of the 2D fractional quantum Hall state [32,33]. However, most previous 1D studies have focused on the flat bands with an unit winding number. To explore the new physics associated with higher winding number flat bands remains unclear and stands as an obstacle to explore.

* Corresponding author.
E-mail addresses: max.arzamasov@me.com (M. Arzamasovs), liubophy@gmail.com (B. Liu).

[1] These authors contribute equally to this work.

https://doi.org/10.1016/j.aop.2024.169837
Received 18 August 2024; Accepted 29 October 2024
Available online 8 November 2024

Here we report the discovery of a new mechanism to achieve the topological flat band with higher winding number in a superradiance lattice. We shall introduce this with a specific model of ultracold atoms, to be illustrated below. The key idea here is to design the non-trivial beyond-nearest-neighbor hopping of atoms in momentum space through our proposed five-level M-type scheme. Surprisingly, it is shown that through tuning the intensities of the coupling fields, the tunneling between atoms in momentum space is highly tunable and the flat band with higher winding number can be achieved. This idea is motivated by the recent experimental progresses in developing the momentum space lattice composed by the timed Dicke states, i.e., superradiance lattices [34–40], which are the collective atomic excitations with phase correlations. Such phase correlations can be recognized as the momenta of the collective excitations. When they satisfy the phase-matching condition, there are directional superradiant light emissions, which can be utilized as one of the remarkable advantages to explore interesting physics in superradiance lattices, such as chiral current [36,38], flat band localization [39], and floquet physics [41]. As we shall show with the model below, our proposed five-level M-type scheme can lead to the flat band with higher winding number.

2. Effective model

Let us take ^{87}Rb atomic system as an example to show our proposed five-level M-type scheme, which is schematically presented in Fig. 1. There are two excited states $|f\rangle = |F=1, m_F=0\rangle$, $|d\rangle = |F=1, m_F=1\rangle$, which can be selected from $5P_{1/2}$ state and $5P_{3/2}$ state, respectively. And $|g\rangle$, $|e\rangle$, $|m\rangle$ can be chosen from $5S_{1/2}$ state, such as $|F=1, m_F=0\rangle$, $|F=2, m_F=0\rangle$ and $|F=2, m_F=2\rangle$. The probe field $\mathbf{E_p}$ and signal field $\mathbf{E_s}$ couple the states $|g\rangle$ and $|f\rangle$, $|e\rangle$ and $|f\rangle$, respectively. Δ_p and Δ_s denote the corresponding frequency detunings. There are two far off-resonant coupling fields $\mathbf{E_c}$ and $\mathbf{E_f}$, where $\mathbf{E_c}$ spontaneously drives both transitions between $|e\rangle$ and $|d\rangle$, $|m\rangle$ and $|d\rangle$, since here $|e\rangle$ and $|m\rangle$ are assumed to be degenerated and the corresponding Rabi frequencies are labeled by Ω_{c_1} and Ω_{c_2}, respectively. $\mathbf{E_f}$ also spontaneously drives both transitions between $|e\rangle$ and $|d\rangle$, $|m\rangle$ and $|d\rangle$, where the corresponding Rabi frequencies are defined as Ω_{f_1} and Ω_{f_2}, respectively. Δ describes the frequency detuning of the above transitions. $\mathbf{k_{p(s,c,f)}}$ are the wave vectors of the corresponding fields, respectively. Since Δ is much larger than other detunings and Rabi frequencies, we can adiabatically eliminate the state $|d\rangle$ and obtain the effective Hamiltonian (see details in Appendix) in the interaction picture as (we set $\hbar = 1$)

$$\begin{aligned}
H =& \sum_n \frac{1}{\Delta}\left(\Omega_{c_1}^2 + \Omega_{f_1}^2 + 2\Omega_{c_1}\Omega_{f_1}\cos k_0 x_n\right)|e_n\rangle\langle e_n| \\
&+ \sum_n \frac{1}{\Delta}\left(\Omega_{c_2}^2 + \Omega_{f_2}^2 + 2\Omega_{c_2}\Omega_{f_2}\cos k_0 x_n\right)|m_n\rangle\langle m_n| \\
&- \sum_n \Delta_{ps}(|e_n\rangle\langle e_n| + |m_n\rangle\langle m_n|) - \Delta_p|f_n\rangle\langle f_n| \\
&+ \sum_n [\frac{1}{\Delta}(\Omega_{c_1}\Omega_{c_2} + \Omega_{f_1}\Omega_{f_2} + \Omega_{c_2}\Omega_{f_1}e^{ik_0x_n} \\
&+ \Omega_{c_1}\Omega_{f_2}e^{-ik_0x_n})|e_n\rangle\langle m_n| + \Omega_p e^{-i\mathbf{k_p}\cdot\mathbf{r_n}}|g_n\rangle\langle f_n| \\
&+ \Omega_s e^{-i\mathbf{k_s}\cdot\mathbf{r_n}}|e_n\rangle\langle f_n| + h.c.]
\end{aligned} \tag{1}$$

where $k_0 = |\mathbf{k_c} - \mathbf{k_f}|$ and $\Delta_{ps} = \Delta_p - \Delta_s$. $\mathbf{r_n}$ labels the coordinate of the nth atom and x_n is the x-component of $\mathbf{r_n}$, where the direction of the x-axis is determined by $\mathbf{k_c} - \mathbf{k_f}$. $|e(g,f,m)_n\rangle$ represents the state $|e(g,f,m)\rangle$ of the atom located at $\mathbf{r_n}$.

By introducing the following operators associated with timed Dicke states in the Dirac notation [42] $\hat{f}_j^\dagger = 1/\sqrt{N}\sum_n e^{i[\mathbf{k_p}+j(\mathbf{k_c}-\mathbf{k_f})]\cdot\mathbf{r_n}}|f_n\rangle\langle g_n|$, $\hat{e}_j^\dagger = 1/\sqrt{N}\sum_n e^{i[\mathbf{k_p}-\mathbf{k_s}+j(\mathbf{k_c}-\mathbf{k_f})]\cdot\mathbf{r_n}}|e_n\rangle\langle g_n|$, $\hat{m}_j^\dagger = 1/\sqrt{N}\sum_n e^{i[\mathbf{k_p}-\mathbf{k_s}+(j-1)(\mathbf{k_c}-\mathbf{k_f})]\cdot\mathbf{r_n}}|m_n\rangle\langle g_n|$ with N being the total number of atoms, the Hamiltonian in Eq. (1) can be transformed to a tight-binding model, $H = H_s + H_p$, where

$$\begin{aligned}
H_s =& \sum_j \varepsilon_e \hat{e}_j^\dagger \hat{e}_j + \varepsilon_m \hat{m}_j^\dagger \hat{m}_j + \sum_j (t_0 \hat{m}_j^\dagger \hat{e}_j + t_1 \hat{m}_{j+1}^\dagger \hat{e}_j \\
&+ t_2 \hat{m}_{j+2}^\dagger \hat{e}_j + t_3 \hat{e}_{j+1}^\dagger \hat{e}_j + t_4 \hat{m}_{j+1}^\dagger \hat{m}_j + h.c.)
\end{aligned} \tag{2}$$

and $H_p = (\sqrt{N}\Omega_p \hat{f}_0 + \sum_j \Omega_s \hat{e}_j^\dagger \hat{f}_j + h.c.) - \sum_j \Delta_p \hat{f}_j^\dagger \hat{f}_j + \Delta_{ps}(\hat{e}_j^\dagger \hat{e}_j + \hat{m}_j^\dagger \hat{m}_j)$, where $\varepsilon_e = (\Omega_{c_1}^2 + \Omega_{f_1}^2)/\Delta$, $\varepsilon_m = (\Omega_{c_2}^2 + \Omega_{f_2}^2)/\Delta$, $t_0 = \Omega_{f_1}\Omega_{c_2}/\Delta$, $t_1 = (\Omega_{c_1}\Omega_{c_2} + \Omega_{f_1}\Omega_{f_2})/\Delta$, $t_2 = \Omega_{c_1}\Omega_{f_2}/\Delta$, $t_3 = \Omega_{c_1}\Omega_{f_1}/\Delta$ and $t_4 = \Omega_{c_2}\Omega_{f_2}/\Delta$.

As shown in Fig. 1(b), t_0 and t_1 describe the hoppings between nearest-neighbor sites within and inbetween the unit cells, respectively. t_2, t_3 and t_4 stands for the distinct beyond-nearest-neighbor hopping amplitudes, respectively. More interestingly, in our proposed five-level M-type scheme, all the hopping amplitudes are highly tunable, which can be achieved through varying the Rabi frequencies and detunings. Therefore, various types of Su-Schrieffer-Heeger (SSH) model, including the standard SSH and extended SSH model [43–47], can be realized. To gain more insight, we rewrite H_s in the real space [36,38] as

$$\tilde{H}_s = h_x\sigma_x + h_y\sigma_y + h_z\sigma_z + h_0 I \tag{3}$$

where $h_x = t_0 + t_1\cos\tilde{k}_x + t_2\cos 2\tilde{k}_x$, $h_y = t_1\sin\tilde{k}_x + t_2\sin 2\tilde{k}_x$, $h_z = (\varepsilon_e - \varepsilon_m)/2 + (t_3 - t_4)\cos\tilde{k}_x$, $h_0 = (\varepsilon_e + \varepsilon_m)/2 + (t_3 + t_4)\cos\tilde{k}_x$ and $\tilde{k}_x = k_0 x$. I is the unit matrix and $\boldsymbol{\sigma}$ is the Pauli's matrix. Through diagonalizing Eq. (3), the band dispersion $E^s(\tilde{k}_x)$ can be obtained as $E_+^s = \frac{1}{\Delta}\sum_{i=1,2}\Omega_{c_i}^2 + \Omega_{f_i}^2 + 2\Omega_{c_i}\Omega_{f_i}\cos\tilde{k}_x$ and $E_-^s = 0$. Surprisingly, it is shown that the corresponding energy bands exhibit that there is a robust flat band for any Rabi frequency and detuning in our five-level M-type scheme. To further consider realizing a

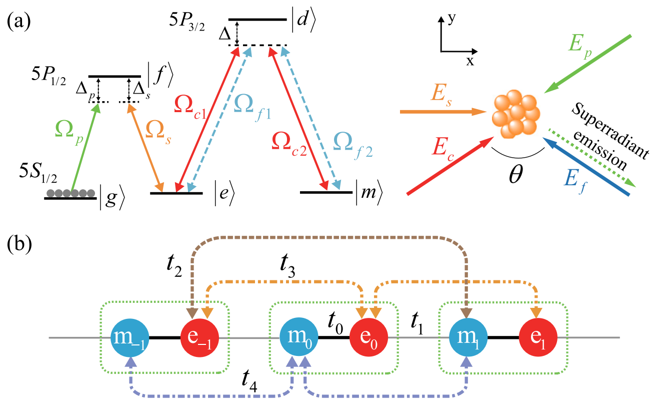

Fig. 1. (a) The schematic plot of our proposed five-level M-type scheme. The coupling fields $\mathbf{E_c}$ and $\mathbf{E_f}$ drive the transition between $|e\rangle$ and $|m\rangle$. The direction of the x-axis is determined by $\mathbf{k_c} - \mathbf{k_f}$. The superradiant beam is marked by the dashed line. (b) The 1D bipartite superradiance lattice in momentum space. t_0 and t_1 stand for the hopping between nearest-neighbor sites within and inbetween the unit cells. t_2, t_3 and t_4 describe the distinct beyond-nearest-neighbor hopping amplitudes, respectively. When varying the Rabi frequencies and detunings in our proposed M-type scheme, all the hopping amplitudes can be changed. Various types of Su-Schrieffer-Heeger (SSH) model, including the standard SSH and extended SSH model, can thus be achieved.

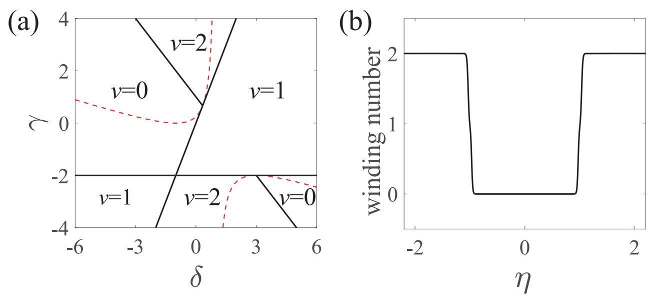

Fig. 2. (a) The topological phase diagram of the model Hamiltonian in Eq. (4). Since here $\Omega/\bar{\Omega} \equiv \eta$ (defined in the main text) is the allowed tuning parameter, the model in Eq. (4) can approach the regime along the red line. (b) The topological phase transition between topological trivial regime with winding number $\nu = 0$ and topological non-trivial regime with winding number $\nu = 2$ when varying η.

two-band Z-type topological system from the model in Eq. (3), we consider tuning the Rabi frequencies satisfying the following relations $\Omega_{c_1} = \Omega_{f_2} \equiv \Omega$ and $\Omega_{c_2} = \Omega_{f_1} \equiv \bar{\Omega}$. Therefore $\tilde{H}_s$ in Eq. (3) can be simplified as

$$\tilde{H}_s' = h_x\sigma_x + h_y\sigma_y + h_0 I \tag{4}$$

where $h_x = (\bar{\Omega}^2 + 2\Omega\bar{\Omega}\cos\tilde{k}_x + \Omega^2\cos 2\tilde{k}_x)/\Delta$, $h_y = (2\Omega\bar{\Omega}\sin\tilde{k}_x + \Omega^2\sin 2\tilde{k}_x)/\Delta$, $h_0 = (\Omega^2 + \bar{\Omega}^2 + 2\Omega\bar{\Omega}\cos\tilde{k}_x)/\Delta$. The corresponding band structure can be determined by $E_+^s = 2(\Omega^2 + \bar{\Omega}^2 + 2\Omega\bar{\Omega}\cos\tilde{k}_x)/\Delta$ and $E_-^s = 0$. From Eq. (4), it is shown that $\Omega/\bar{\Omega} \equiv \eta$ is the allowed tuning parameter here. Therefore, the Hamiltonian parameters $\delta \equiv (t_1 - t_0)/(t_0 + t_1)$ and $\gamma \equiv 2t_2/(t_0 + t_1)$ are constrained by the following relation $\delta/\gamma = (2\eta - 1)/2\eta^2$. As shown in Fig. 2(a), such a constrain will effect the topological properties of the system.

Since the system belongs to Z-type, the typological nature can be characterized by the winding number defined as $\nu = \frac{1}{2\pi}\oint_C \frac{h_x dh_y - h_y dh_x}{h_x^2 + h_y^2}$, where C stands for $\tilde{k}_x$ varying from 0 to 2π. We find that the model in Eq. (4) can approach the topological regime along the red line in Fig. 2(a). There is a topological phase transition from the topological trivial regime with $\nu = 0$ to the topological non-trivial regime with $\nu = 2$ when varying η as shown in Fig. 2(b). More interestingly, we find that when the system in the topological regime, the flat band also shows the non-trivial topological property, which is characterized by a higher winding number $w = \frac{1}{\pi}\int_0^{2\pi} d\tilde{k}_x \langle\psi|i\partial_{\tilde{k}_x}|\psi\rangle$ being 2, where $|\psi\rangle$ is eigen-state of Eq. (4) corresponding to the flat band (see details in Appendix).

3. Superradiance spectra

The above topological phase transition can be detected through the superradiance spectra, which will reflect the changes in the band structure [34–36,39,40]. Distinct from the spontaneous radiation, superradiance emission is a collective effect and generates a stronger directional radiance. By setting the phase matching condition as $|\mathbf{k_p}+\mathbf{k_c}-\mathbf{k_f}| = |\mathbf{k_p}|$, superradiance photon will be emitted along the direction determined by $\mathbf{k_p}+\mathbf{k_c}-\mathbf{k_f}$, which is indicated by the dashed line in Fig. 1(a). The intensity of superradiance emission can be calculated by solving the following master equation

$$-i[H,\rho]+\sum_{\alpha}\Gamma_{\alpha}\left(L_{\alpha}\rho L_{\alpha}^{\dagger}-\frac{1}{2}\{L_{\alpha}^{\dagger}L_{\alpha},\rho\}\right)=0 \tag{5}$$

where α runs over p,s,c,f and Γ_{α} describes the corresponding transition decay rate. L_{α} is the Linblad operator defined as $L_p=\sum_j|g\rangle\langle f_j|$, $L_s=\sum_j|e_j\rangle\langle f_j|$, $L_c=\sum_j|e_j\rangle\langle d_j|$ and $L_f=\sum_j|m_j\rangle\langle d_j|$, respectively. Since both the probe and signal fields are weak, atoms are mainly populated at the ground state $|g\rangle$. Then, the density matrix can be expressed as $\rho=|g\rangle\langle g|+\sum_j(A_j|e_j\rangle\langle g|+\sum_j B_j|m_j\rangle\langle g|+\sum_j C_j|f_j\rangle\langle g|+h.c.)$. Substituting the above expression of density matrix into Eq. (5), we obtain the following equation for the steady state

$$\begin{pmatrix} & & & & \cdots & & & \\ t_0 & \Delta_2-\Delta_{ps} & 0 & t_4 & 0 & 0 & 0 & 0\\ t_3 & 0 & \Delta_1-\Delta_{ps} & t_0 & t_3 & t_1 & 0 & t_2\\ t_1 & t_4 & t_0 & \Delta_2-\Delta_{ps} & 0 & t_4 & 0 & 0\\ 0 & 0 & t_3 & 0 & \Delta_1-\Delta_{ps} & t_0 & t_3 & t_1\\ t_2 & 0 & t_1 & t_4 & t_0 & \Delta_2-\Delta_{ps} & 0 & t_4\\ 0 & 0 & 0 & 0 & t_3 & 0 & \Delta_1-\Delta_{ps} & t_0\\ & & & & \cdots & & & \end{pmatrix}\begin{pmatrix}\cdots\\ B_{-1}\\ A_0\\ B_0\\ A_1\\ B_1\\ A_2\\ \cdots\end{pmatrix}=\begin{pmatrix}\cdots\\ 0\\ -\frac{\Omega_p\Omega_s}{\Delta_p+i\Gamma}\\ 0\\ 0\\ 0\\ 0\\ \cdots\end{pmatrix} \tag{6}$$

where $\Delta_1=\Delta_2+|\Omega_s|^2/(\Delta_p+i\Gamma)$, $\Delta_2=(\Omega^2+\bar{\Omega}^2)/\Delta$, and Γ is the decay rate of $|f\rangle$. Note that under the condition $\Omega_p\ll\Omega,\bar{\Omega}$, it is found that C_j depends linearly on A_j through the relation $C_j=(\Omega_sA_j+\Omega_p\delta_{j,0})/(\Delta_p+i\Gamma)$. Through solving the density matrix for the steady state from Eq. (6), the electric polarization intensity of atoms can be calculated via the following relation $\mathbf{P}=-e\mathrm{Tr}[U^{\dagger}\rho U\mathbf{r}]=\mathbf{P}_pe^{-i\omega_pt}+\mathbf{P}_{ps}e^{-i(\omega_p-\omega_s)t}+c.c.$, where $U=\exp(-iH_0t)$ with $H_0=-\sum_j\omega_p|f_j\rangle\langle f_j|+(\omega_p-\omega_s)(|e_j\rangle\langle e_j|+|m_j\rangle\langle m_j|)$ (see details in Appendix). Then, the susceptibility of atomic medium can be obtained from the following relation

$$\chi=P_p/\varepsilon_0E_pe^{i\mathbf{k_p}\cdot\mathbf{r}}=\sum_j\chi_je^{ij(\mathbf{k_c}-\mathbf{k_f})\cdot\mathbf{r}} \tag{7}$$

where P_p is the amplitude of $\mathbf{P}_p$ and $\chi_j=\mu_{fg}C_j/\varepsilon_0E_pV$ with μ_{fg} being the electric dipole matrix element related to the atomic transition between $|f\rangle$ and $|g\rangle$. E_p is the field amplitude of the incident probe beam. V is the volume of atom ensemble and ε_0 is permittivity of vacuum. The reflectivity R can be calculated through the following equations [35,38]

$$\begin{aligned}\partial_xE_p&=-\beta_0E_p+i\kappa_{-1}e^{-ik_0x}E_r\\ \partial_xE_r&=\beta_0E_r-i\kappa_{+1}e^{ik_0x}E_p\end{aligned} \tag{8}$$

where $\beta_0=\frac{\omega_p^2}{2k_pc^2\sin\frac{\theta}{2}}\mathrm{Im}(\chi_0)$ and $\kappa_{\pm1}=\frac{\omega_p^2}{2k_pc^2\sin\frac{\theta}{2}}\chi_{\pm1}$. E_r is the field amplitude of the scattered beam, i.e. superradiance emission. The reflectivity $R=|E_r(0)/E_p(0)|^2$, under the boundary condition $E_p(0)=E_0$, $E_r(L)=0$, can be solved though the following relation

$$R=\left|\frac{\kappa_{+1}(e^{-\lambda L}-e^{\lambda L})}{(\beta-\lambda)e^{-\lambda L}-(\beta+\lambda)e^{\lambda L}}\right|^2 \tag{9}$$

where $\beta=\beta_0-\frac{i}{2}k_0$ and $\lambda=\sqrt{\beta^2+\kappa_{+1}\kappa_{-1}}$. L is the length of the system along the x-axis. From Eq. (9), it is found that $R\propto A_1$. And A_1 can be obtained from Eq. (6), which satisfies the relation $A_1(\Delta_{ps})\propto\mathrm{Dos}(E^s)|_{E^s=\Delta_{ps}}$ with $\mathrm{Dos}(E^s)$ being the density of state of the band spectra $E^s(\tilde{k}_x)$ of the Hamiltonian $\tilde{H}_s'$. Therefore, when Δ_{ps} approaching the energy where $\mathrm{Dos}(E^s)$ diverges, there should be a peak at the intensity of superradiant emission. As shown in Fig. 3, all the peaks of the intensity of superradiant emission are located at the saddle point of the energy spectra $E^s(\tilde{k}_x)$. The top and bottom of each energy band of H_s can thus be determined. As shown in Fig. 3 from top line to bottom line, when varying η, there is a topological phase transition. At the transition point, the system becomes gapless. It can be detected from counting the peaks of the intensity of superradiant emission. As shown in Fig. 3(d), there are only two peaks in R, indicating that the energy gap is closed and the topological phase transition occurs. Therefore, the topological phase diagram as shown in Fig. 2(b) can be determined.

4. Conclusion

In summary, we propose a five-level M-type scheme in atomic ensembles to induce a 1D bipartite superradiance lattice in momentum space. Such a lattice shows great tunability of changing both the nearest-neighbor and beyond-nearest-neighbor hopping amplitude through varying the Rabi frequencies and detunings. Various types of SSH models can thus be achieved and a flat band with higher winding number can be found. We also proposed that the superradiance spectra can be utilized as a tool for experimental detection. Our proposal would provide a promising approach to explore the new physics in the flat bands with higher topological number.

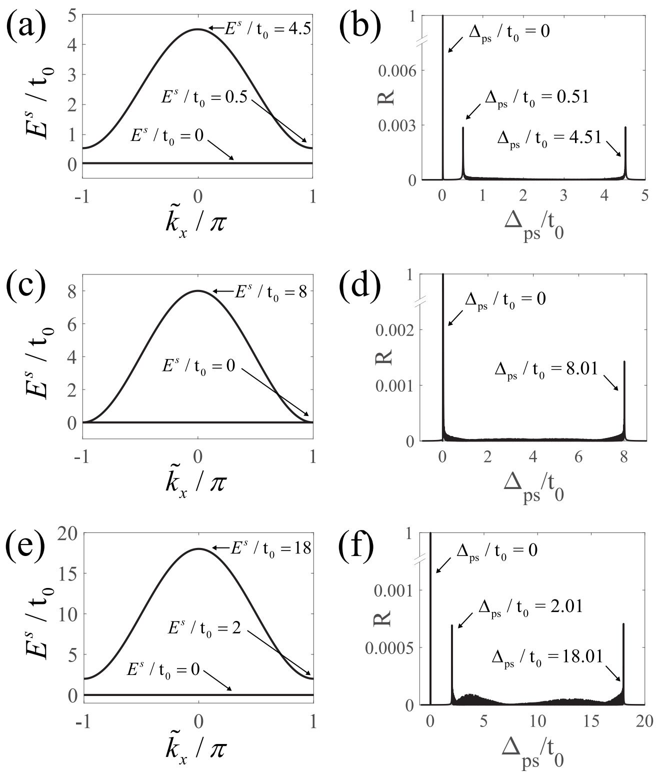

Fig. 3. Energy spectra of the Hamiltonian $\tilde{H}'_s$ (left column) vs. superradiance emission spectra (right column) for different η: (a)(b) $\eta = 0.5$, (c)(d) $\eta = 1.0$ and (e)(f) $\eta = 2$. It is shown that both the top and bottom of each energy band of $\tilde{H}'_s$ can be determined by the locations of the peaks of the intensity of superradiance emission.

CRediT authorship contribution statement

Shuai Li: Performed all calculations under the supervision of M.A. and B.L.. **Rui Tian:** Performed all calculations under the supervision of M.A. and B.L.. **Min Liu:** Performed calculations and contributed in completing the paper. **Maksims Arzamasovs:** Worked on theoretical analysis and contributed in completing the paper. **Liangchao Chen:** Worked on experimental proposal and contributed in completing the paper. **Bo Liu:** Proposed the study, worked on theoretical analysis and contributed in completing the paper..

Declaration of competing interest

The authors declare that they have no known competing financial interests or personal relationships that could have appeared to influence the work reported in this paper.

Acknowledgments

This work is supported by the National Key R&D Program of China (2021YFA1401700), NSFC, China (Grants No. 12074305, 12474267), the Fundamental Research Funds for the Central Universities, China (Grant No. xtr052023002), Shaanxi Fundamental Science Research Project for Mathematics and Physics, China (Grant No. 23JSZ003) (S. L., R. T., M. L., M. A. and B. L.) and NSFC, China (Grant No. 12004229) (L. C.). We also thank the HPC platform of Xi'An Jiaotong University, where our numerical calculation was performed.

Appendix A. Effective model

The Hamiltonian of an ensemble of 5-level M-type coupled system as shown in Fig. 1(a) can be expressed as (we set $\hbar = 1$)

$$\begin{aligned}H_S =&H_0 + \sum_n \omega_{fg}|f_n\rangle\langle f_n| + \omega_{eg}|e_n\rangle\langle e_n| + \omega_{dg}|d_n\rangle\langle d_n| + \omega_{mg}|m_n\rangle\langle m_n|\\ &+2\Big\{ \Omega_p \cos(\mathbf{k_p}\cdot\mathbf{r_n} - \omega_p t)|g_n\rangle\langle f_n| + \Omega_s\cos(\mathbf{k_s}\cdot\mathbf{r_n}-\omega_s t)|e_n\rangle\langle f_n|\\ &+[\Omega_{c_1}\cos(\mathbf{k_c}\cdot\mathbf{r_n}-\omega_c t) + \Omega_{f_1}\cos(\mathbf{k_f}\cdot\mathbf{r_n}-\omega_f t)]|e_n\rangle\langle d_n|\\ &+[\Omega_{c_2}\cos(\mathbf{k_c}\cdot\mathbf{r_n}-\omega_c t) + \Omega_{f_2}\cos(\mathbf{k_f}\cdot\mathbf{r_n}-\omega_f t)]|m_n\rangle\langle d_n| + h.c.\Big\}\end{aligned} \tag{A.1}$$

where $\omega_{f(e,d,m)g}$ is the energy difference between $|f(e,d,m)\rangle$ and $|g\rangle$, respectively and H_0 is the kinetic energy of the free moving atom. $\mathbf{r_n}$ labels the coordinate of the nth atom. $\mathbf{k_{p(s,c,f)}}$ and $\omega_{p(s,c,f)}$ are the wave vector and frequency of the corresponding laser fields and the respective Rabi frequencies are denoted as $\Omega_{p(s,c_1,c_2,f_1,f_2)}$, respectively. By transforming the Hamiltonian to a rotating frame, we obtain the Hamiltonian in the interaction picture

$$\begin{aligned}H_I =&e^{iH_1t}H_S e^{-iH_1t} - H_1\\ =&H_0+\Big[\sum_n \Omega_p e^{-i\mathbf{k_p}\cdot\mathbf{r_n}+i\Delta_p t}|g_n\rangle\langle f_n| + \Omega_s e^{-i\mathbf{k_s}\cdot\mathbf{r_n}+i\Delta_s t}|e_n\rangle\langle f_n|\\ &+(\Omega_{c_1}e^{-i\mathbf{k_c}\cdot\mathbf{r_n}} + \Omega_{f_1}e^{-i\mathbf{k_f}\cdot\mathbf{r_n}})e^{i\Delta t}|e_n\rangle\langle d_n| + (\Omega_{c_2}e^{-i\mathbf{k_c}\cdot\mathbf{r_n}} + \Omega_{f_2}e^{-i\mathbf{k_f}\cdot\mathbf{r_n}})e^{i\Delta t}|m_n\rangle\langle d_n| + h.c.\Big],\end{aligned} \tag{A.2}$$

where $\Delta_p \equiv \omega_p - \omega_{fg}$, $\Delta_s \equiv \omega_s - (\omega_{fg} - \omega_{eg})$, $\Delta \equiv \omega_c - (\omega_{dg} - \omega_{eg}) = \omega_f - (\omega_{dg} - \omega_{mg})$ are the corresponding detunings and $H_1 = \sum_n \omega_{fg}|f_n\rangle\langle f_n| + \omega_{eg}|e_n\rangle\langle e_n| + \omega_{dg}|d_n\rangle\langle d_n| + \omega_{mg}|m_n\rangle\langle m_n|$. Considering the case with $\omega_c = \omega_f$, $\omega_{eg} = \omega_{mg}$ and Δ is much larger than other detunings and Rabi frequencies, we can adiabatically eliminate the state $|d\rangle$ and rewrite the Hamiltonian in Eq. (A.2) as

$$\begin{aligned}H_I =&H_0 + \sum_n \frac{1}{\Delta}\left(\Omega_{c_1}^2 + \Omega_{f_1}^2 + 2\Omega_{c_1}\Omega_{f_1}\cos[(\mathbf{k_c}-\mathbf{k_f})\cdot\mathbf{r_n}]\right)|e_n\rangle\langle e_n|\\ &+\frac{1}{\Delta}\left(\Omega_{c_2}^2 + \Omega_{f_2}^2 + 2\Omega_{c_2}\Omega_{f_2}\cos[(\mathbf{k_c}-\mathbf{k_f})\cdot\mathbf{r_n}]\right)|m_n\rangle\langle m_n|\\ &+\Big[\frac{1}{\Delta}\left(\Omega_{c_1}\Omega_{c_2} + \Omega_{f_1}\Omega_{f_2} + \Omega_{c_2}\Omega_{f_1}e^{i(\mathbf{k_c}-\mathbf{k_f})\cdot\mathbf{r_n}} + \Omega_{c_1}\Omega_{f_2}e^{-i(\mathbf{k_c}-\mathbf{k_f})\cdot\mathbf{r_n}}\right)|e_n\rangle\langle m_n|\\ &+\Omega_p e^{-i\mathbf{k_p}\cdot\mathbf{r_n}+i\Delta_p t}|g_n\rangle\langle f_n| + \Omega_s e^{-i\mathbf{k_s}\cdot\mathbf{r_n}+i\Delta_s t}|e_n\rangle\langle f_n| + h.c.\Big]\end{aligned} \tag{A.3}$$

Then, another transformation is applied to the Hamiltonian in Eq. (A.3) and we obtained that

$$\begin{aligned}H =&e^{iH_2t}H_I e^{-iH_2t} - H_2\\ =&H_0 + \sum_n -\Delta_p|f_n\rangle\langle f_n| - (\Delta_p - \Delta_s)(|e_n\rangle\langle e_n| + |m_n\rangle\langle m_n|)\\ &+\frac{1}{\Delta}\left(\Omega_{c_1}^2 + \Omega_{f_1}^2 + 2\Omega_{c_1}\Omega_{f_1}\cos k_0x_n\right)|e_n\rangle\langle e_n|\\ &+\frac{1}{\Delta}\left(\Omega_{c_2}^2 + \Omega_{f_2}^2 + 2\Omega_{c_2}\Omega_{f_2}\cos k_0x_n\right)|m_n\rangle\langle m_n|\\ &+\Big[\frac{1}{\Delta}\left(\Omega_{c_1}\Omega_{c_2} + \Omega_{f_1}\Omega_{f_2} + \Omega_{c_2}\Omega_{f_1}e^{ik_0x_n} + \Omega_{c_1}\Omega_{f_2}e^{-ik_0x_n}\right)|e_n\rangle\langle m_n|\\ &+\Omega_p e^{-i\mathbf{k_p}\cdot\mathbf{r_n}}|g_n\rangle\langle f_n| + \Omega_s e^{-i\mathbf{k_s}\cdot\mathbf{r_n}}|e_n\rangle\langle f_n| + h.c.\Big],\end{aligned} \tag{A.4}$$

where $H_2 = \sum_n \Delta_p|f_n\rangle\langle f_n| + (\Delta_p - \Delta_s)(|e_n\rangle\langle e_n| + |m_n\rangle\langle m_n|)$ and $k_0 = |\mathbf{k_c} - \mathbf{k_f}|$. To construct the tight binding model, we rewrite Eq. (A.4) in the bases of $|e_j\rangle_\mathbf{k}$ and $|m_j\rangle_\mathbf{k}$, where $|e_j\rangle_\mathbf{k} = \frac{1}{\sqrt{N}}\sum_n \exp\{i[\mathbf{k} + \mathbf{k_p} - \mathbf{k_s} + j(\mathbf{k_c} - \mathbf{k_f})]\cdot\mathbf{r_n}\}|e_n\rangle$ and $|m_j\rangle_\mathbf{k} = \frac{1}{\sqrt{N}}\sum_n \exp\{i[\mathbf{k} + \mathbf{k_p} - \mathbf{k_s} + (j-1)(\mathbf{k_c} - \mathbf{k_f})]\cdot\mathbf{r_n}\}|m_n\rangle$, with $\mathbf{k}$ being the initial momentum of atoms. Then, the tight-binding model can be expressed as

$$H_{TB} = \tilde{H}_K(\mathbf{k}) + \tilde{H}_s(\mathbf{k}), \tag{A.5}$$

where $\tilde{H}_K = \sum_j \frac{[\mathbf{k}+\mathbf{k_p}-\mathbf{k_s}+j(\mathbf{k_c}-\mathbf{k_f})]^2}{2m}|e_j\rangle_\mathbf{k}\langle e_j|_\mathbf{k} + \frac{[\mathbf{k}+\mathbf{k_p}-\mathbf{k_s}+(j-1)(\mathbf{k_c}-\mathbf{k_f})]^2}{2m}|m_j\rangle_\mathbf{k}\langle m_j|_\mathbf{k}$ and $\tilde{H}_s = \frac{1}{\Delta}\sum_j(\Omega_{c_1}^2 + \Omega_{f_1}^2)|e_j\rangle_\mathbf{k}\langle e_j|_\mathbf{k} + (\Omega_{c_2}^2 + \Omega_{f_2}^2)|m_j\rangle_\mathbf{k}\langle m_j|_\mathbf{k} + [\Omega_{f_1}\Omega_{c_2}|m_j\rangle_\mathbf{k}\langle e_j|_\mathbf{k} + (\Omega_{c_1}\Omega_{c_2} + \Omega_{f_1}\Omega_{f_2})|m_{j+1}\rangle_\mathbf{k}\langle e_j|_\mathbf{k} + \Omega_{c_1}\Omega_{f_2}|m_{j+2}\rangle_\mathbf{k}\langle e_j|_\mathbf{k} + \Omega_{c_1}\Omega_{f_1}|e_{j+1}\rangle_\mathbf{k}\langle e_j|_\mathbf{k} + \Omega_{c_2}\Omega_{f_2}|m_{j+1}\rangle_\mathbf{k}\langle m_j|_\mathbf{k} + h.c.]$. H_{TB} in Eq. (A.5) can further be written in the matrix form

$$\Psi^\dagger\begin{pmatrix} & & & \cdots & & & & \\ 0 & E_r(k+1)^2+\varepsilon_e & t_0 & t_3 & t_1 & 0 & t_2 & 0\\ t_4 & t_0 & E_rk^2+\varepsilon_m & 0 & t_4 & 0 & 0 & 0\\ 0 & t_3 & 0 & E_rk^2+\varepsilon_e & t_0 & t_3 & t_1 & 0\\ 0 & t_1 & t_4 & t_0 & E_r(k-1)^2+\varepsilon_m & 0 & t_4 & 0\\ 0 & 0 & 0 & t_3 & 0 & E_r(k-1)^2+\varepsilon_e & t_0 & t_3\\ 0 & t_2 & 0 & t_1 & t_4 & t_0 & E_r(k-2)^2+\varepsilon_m & 0\\ & & & \cdots & & & & \end{pmatrix}\Psi, \tag{A.6}$$

where $\Psi^\dagger = (\ldots, |e_1\rangle_\mathbf{k}, |m_1\rangle_\mathbf{k}, |e_0\rangle_\mathbf{k}, |m_0\rangle_\mathbf{k}, |e_{-1}\rangle_\mathbf{k}, |m_{-1}\rangle_\mathbf{k}, \ldots)$, $E_r = |\mathbf{k_c} - \mathbf{k_f}|^2/2m$, and $k = (\mathbf{k} + \mathbf{k_p} - \mathbf{k_s})\cdot\hat{\mathbf{e}}_{\mathbf{k_c}-\mathbf{k_f}}/|\mathbf{k_c} - \mathbf{k_f}|$ with $\hat{\mathbf{e}}_{\mathbf{k_c}-\mathbf{k_f}} \equiv (\mathbf{k_c} - \mathbf{k_f})/|\mathbf{k_c} - \mathbf{k_f}|$. Such a Hamiltonian thus describes a one-dimensional tight-binding lattice in the momentum space, where $t_{0(1,2,3,4)}$

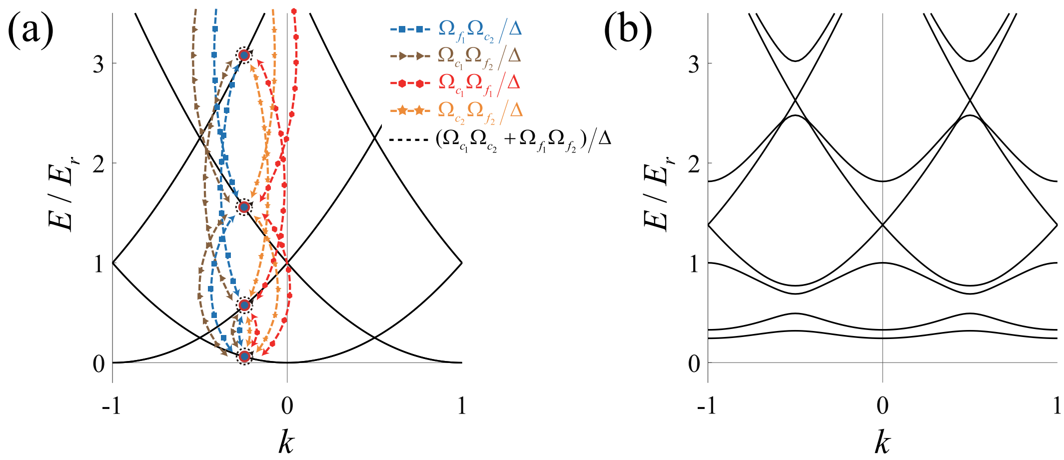

Fig. 4. (a) Solid line shows the free particle dispersion relation. Different atomic states denoted by the blue (red) dots are coupled with each other, where distinct coupling strengths are labeled by the differently colored dashed lines. In our proposed setup as shown in Fig. 1 in the main text, the states with momentum difference $\mathbf{k_c}-\mathbf{k_f}$ are coupled. For example, the states with momentum $(-0.25\pm n)(\mathbf{k_c}-\mathbf{k_f})$ with $n=0,1,2,\ldots$ are shown here. (b) The band structure of our proposed one-dimensional tight-binding lattice, where $t_0=t_2=t_3=t_4=0.2E_r$, $t_1=\varepsilon_e=\varepsilon_m=0.4E_r$ and $k=(\mathbf{k}+\mathbf{k_p}-\mathbf{k_s})\cdot\hat{\mathbf{e}}_{\mathbf{k_c}-\mathbf{k_f}}/|\mathbf{k_c}-\mathbf{k_f}|$ with $\hat{\mathbf{e}}_{\mathbf{k_c}-\mathbf{k_f}}\equiv(\mathbf{k_c}-\mathbf{k_f})/|\mathbf{k_c}-\mathbf{k_f}|$.

describes the distinct hopping amplitudes and the kinetic term is characterized by the harmonic potential in the momentum space. Distinct from the real space lattice, the potential energy and kinetic energy exchange their roles here. $t_{0(1,2,3,4)}$ and $\varepsilon_{e(m)}$ are defined in Eq. (2) in the main text. The band structure of the above Hamiltonian is shown as the function of the momenta k, being the good quantum number here. For instance, in the coupling regime $t<E_r$, with t being the maximal hopping amplitude, the band structure is shown in Fig. 4(b). It is shown that the coupling between different atomic states would remove the band degeneracy and open the band gap.

In this work, we consider the coupling regime $t\gg E_r$. A length scale $\lambda=\sqrt{t/E_r}$ can be defined [34], within which the kinetic energy term is negligible compared with the hopping energy [48–50]. Since the kinetic term can be discarded, the band structure will be not effected by the initial momentum of atoms. Without loss of generality, we thus choose the initial momentum of atoms $\mathbf{k}$ being zero. Through introducing the following bases $|f_j\rangle=\frac{1}{\sqrt{N}}\sum_n\exp\{i[\mathbf{k_p}+j(\mathbf{k_c}-\mathbf{k_f})]\cdot\mathbf{r_n}\}|f_n\rangle$, $|e_j\rangle=\frac{1}{\sqrt{N}}\sum_n\exp\{i[\mathbf{k_p}-\mathbf{k_s}+j(\mathbf{k_c}-\mathbf{k_f})]\cdot\mathbf{r_n}\}|e_n\rangle$ and $|m_j\rangle=\frac{1}{\sqrt{N}}\sum_n\exp\{i[\mathbf{k_p}-\mathbf{k_s}+(j-1)(\mathbf{k_c}-\mathbf{k_f})]\cdot\mathbf{r_n}\}|m_n\rangle$, each term in Eq. (A.4) (kinetic term being discarded) can be rewritten, for instance,

$$\sum_n\frac{1}{\Delta}(\Omega_{c_1}^2+\Omega_{f_1}^2+2\Omega_{c_1}\Omega_{f_1}\cos k_0x_n)|e_n\rangle\langle e_n|=\sum_j\frac{1}{\Delta}[(\Omega_{c_1}^2+\Omega_{f_1}^2)|e_j\rangle\langle e_j|+\Omega_{c_1}\Omega_{f_1}(|e_j\rangle\langle e_{j-1}|+h.c.)] \tag{A.7}$$

$$\begin{aligned}\sum_n\frac{1}{\Delta}(\Omega_{c_1}\Omega_{c_2}+\Omega_{f_1}\Omega_{f_2}+\Omega_{c_2}\Omega_{f_1}e^{ik_0x_n}+\Omega_{c_1}\Omega_{f_2}e^{-ik_0x_n})|e_n\rangle\langle m_n|=\sum_j\frac{1}{\Delta}[(\Omega_{c_1}\Omega_{c_2}+\Omega_{f_1}\Omega_{f_2})|e_j\rangle\langle m_{j+1}|\\+\Omega_{c_2}\Omega_{f_1}|e_j\rangle\langle m_j|+\Omega_{c_1}\Omega_{f_2}|e_j\rangle\langle m_{j+2}|]\end{aligned} \tag{A.8}$$

Therefore, from Eq. (A.4), we can obtain

$$H=H_s+H_p, \tag{A.9}$$

with

$$\begin{aligned}H_s=\frac{1}{\Delta}\sum_j(\Omega_{c_1}^2+\Omega_{f_1}^2)|e_j\rangle\langle e_j|+(\Omega_{c_2}^2+\Omega_{f_2}^2)|m_j\rangle\langle m_j|+[\Omega_{f_1}\Omega_{c_2}|m_j\rangle\langle e_j|+(\Omega_{c_1}\Omega_{c_2}+\Omega_{f_1}\Omega_{f_2})|m_{j+1}\rangle\langle e_j|\\+\Omega_{c_1}\Omega_{f_2}|m_{j+2}\rangle\langle e_j|+\Omega_{c_1}\Omega_{f_1}|e_{j+1}\rangle\langle e_j|+\Omega_{c_2}\Omega_{f_2}|m_{j+1}\rangle\langle m_j|+h.c.]\end{aligned} \tag{A.10}$$

$$H_p=\left(\sqrt{N}\Omega_p|g\rangle\langle f_0|+\sum_j\Omega_s|e_j\rangle\langle f_j|+h.c.\right)-\sum_j\Delta_p|f_j\rangle\langle f_j|+(\Delta_p-\Delta_s)(|e_j\rangle\langle e_j|+|m_j\rangle\langle m_j|) \tag{A.11}$$

Then, our proposed one-dimensional tight-binding lattice in the momentum space can be described by the Hamiltonian H_s, which corresponds to the Eq. (2) in the main text. The band structure in the regime with $t\gg E_r$ is depicted in Fig. 3 in the main text and a topologically robust flat band has been found.

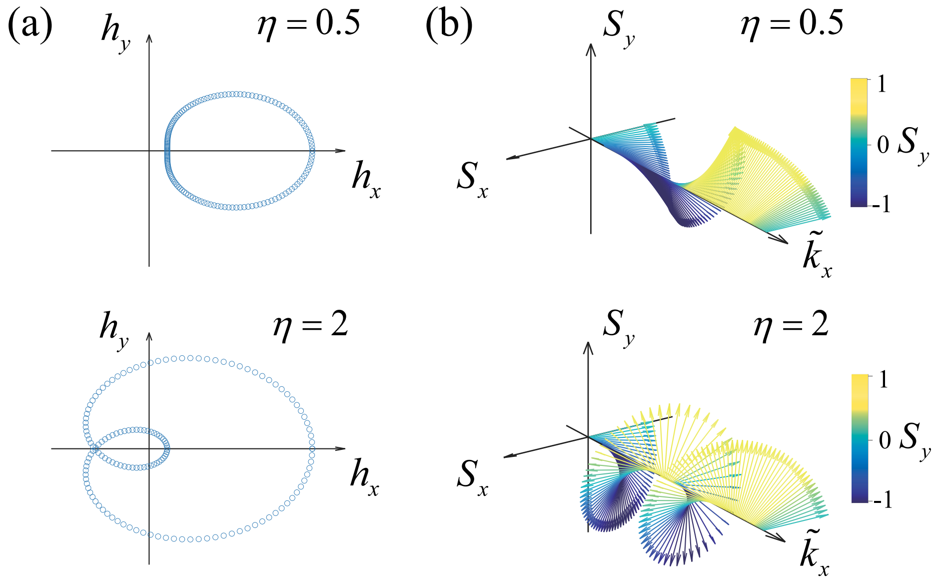

Fig. 5. (a) The winding of the Hamiltonian in Eq. (B.1). (b) The pseudo-spin distributions of the flat bands over the Brillouin Zone. Here the upper and lower panels are for $\eta = 0.5$ and $\eta = 2$, respectively.

Appendix B. Topological nature of the superradiance lattice

Starting from Eq. (2) in the main text, we consider tuning the Rabi frequencies satisfying the following relations $\Omega_{c_1} = \Omega_{f_2} \equiv \Omega$ and $\Omega_{c_2} = \Omega_{f_1} \equiv \bar{\Omega}$ and Eq. (4) in the main text can thus be obtained

$$\tilde{H}_s' = h_x\sigma_x + h_y\sigma_y + h_0 I \tag{B.1}$$

where $h_x = (\bar{\Omega}^2 + 2\Omega\bar{\Omega}\cos\tilde{k}_x + \Omega^2\cos 2\tilde{k}_x)/\Delta$, $h_y = (2\Omega\bar{\Omega}\sin\tilde{k}_x + \Omega^2\sin 2\tilde{k}_x)/\Delta$ and $h_0 = (\Omega^2 + \bar{\Omega}^2 + 2\Omega\bar{\Omega}\cos\tilde{k}_x)/\Delta$. Since the system belongs to Z-type, the typological nature can be characterized by the winding number defined as

$$\nu = \frac{1}{2\pi}\oint_C \frac{h_x dh_y - h_y dh_x}{h_x^2 + h_y^2} \tag{B.2}$$

where C is a close loop with $\tilde{k}_x$ varying from 0 to 2π and $\Omega/\bar{\Omega} \equiv \eta$ is the allowed tuning parameter here. Such a winding number describes the total number of times that the Hamiltonian travels around the origin, which can be any integer and indicates different topological phases. As shown in Fig. 5(a), the winding numbers are 0 and 2 for $\eta = 0.5$ and $\eta = 2$, respectively. It indicates that when varying η there is a topological phase transition from the topological trivial regime to the topological non-trivial regime with higher winding number.

Furthermore, to visualize the topological nontrivial property of the flat band of the Hamiltonian in Eq. (B.1), as shown in Fig. 5(b), the pseudo-spin distribution of the flat band over the Brillouin zone is demonstrated, where the pseudo-spin vector $\mathbf{S}$ is defined as $\mathbf{S} = (S_x, S_y)$ with $S_i = \langle\psi|\sigma_i|\psi\rangle/\langle\psi|\psi\rangle$ and $|\psi\rangle$ being the eigen-state of Eq. (B.1) corresponding to the flat band. It is shown that when varying $\tilde{k}_x$ from 0 to 2π, compared to the topological trivial case with $\eta = 0.5$, the spin vector $\mathbf{S}$ winds an angle of 4π for $\eta = 2$, indicating its topological nontrivial nature. Such distinct behaviors of the spin vector can be characterized by the following winding number

$$\omega_s = \frac{1}{2\pi}\oint_C \frac{S_x dS_y - S_y dS_x}{S_x^2 + S_y^2} \tag{B.3}$$

where $\omega_s = 0$ for $0 < \eta < 1$ and $\omega_s = 2$ for $\eta > 1$, corresponding to the topologically distinct regimes of the flat band.

Appendix C. Superradiance spectra

In this section, we will show the details on how to calculate the intensity of the superradiance emission. The dynamic evolution of our proposed 5-level M-type system can be determined by the following master equation

$$\frac{d\rho}{dt} = -i[H,\rho] + \sum_\alpha \Gamma_\alpha \left(L_\alpha\rho L_\alpha^\dagger - \frac{1}{2}\{L_\alpha^\dagger L_\alpha, \rho\}\right) \tag{C.1}$$

Note that here we consider the regime $t \gg E_r$, the free particle kinetic term can be ignored and H in Eq. (C.1) thus corresponds to the Eq. (2) in the main text. Since both the probe and signal fields are weak, atoms are mainly populated at the ground state $|g\rangle$. The steady state can thus be approximated as $|\psi_s\rangle = |g\rangle + \sum_j A_j|e_j\rangle + B_j|m_j\rangle + C_j|f_j\rangle - O(A^2) - O(B^2) - O(C^2)$ with $|A_j(B_j, C_j)| \ll 1$. Then, the density matrix can be assumed as $\rho = |g\rangle\langle g| + \sum_j (A_j|e_j\rangle\langle g| + B_j|m_j\rangle\langle g| + C_j|f_j\rangle\langle g| + h.c.)$. In the steady state $\dot{\rho} = 0$, Eq. (C.1) can be rewritten as

$$\begin{aligned}&(\Delta_s - \Delta_p + \varepsilon_e)A_j + t_3 A_{j-1} + t_3 A_{j+1} + t_0 B_j + t_1 B_{j+1} + t_2 B_{j+2} + \Omega_s C_j = 0\\&(\Delta_s - \Delta_p + \varepsilon_m)B_j + t_4 B_{j-1} + t_4 B_{j+1} + t_0 A_j + t_1 A_{j-1} + t_2 A_{j-2} = 0\\&-(\Delta_p + i\Gamma)C_j + \Omega_s A_j = -\Omega_p \delta_{j,0}\end{aligned} \tag{C.2}$$

where $\Gamma = (\Gamma_p + \Gamma_s)/2$. Eliminating C_j in Eq. (C.2), we then obtain

$$\begin{aligned}&\left(\frac{\Omega_s^2}{\Delta_p + i\Gamma} + \Delta_s - \Delta_p + \varepsilon_e\right)A_j + t_3 A_{j-1} + t_3 A_{j+1} + t_0 B_j + t_1 B_{j+1} + t_2 B_{j+2} = -\frac{\Omega_p\Omega_s}{\Delta_p + i\Gamma}\delta_{j,0}\\&(\Delta_s - \Delta_p + \varepsilon_m)B_j + t_4 B_{j-1} + t_4 B_{j+1} + t_0 A_j + t_1 A_{j-1} + t_2 A_{j-2} = 0\end{aligned} \tag{C.3}$$

which correspond to Eq. (6) in the main text. Therefore the steady density matrix can be numerically obtained by solving Eq. (C.3).

The density matrix solved above can be used to calculate the electric polarization intensity of atoms, where the polarization can be defined in the Schrödinger picture as

$$\begin{aligned}\mathbf{P} &= -e\mathrm{Tr}[e^{-i(H_1+H_2)t}\rho e^{i(H_1+H_2)t}\mathbf{r}]\\&= \mathbf{P}_p e^{-i\omega_p t} + \mathbf{P}_{ps} e^{-i(\omega_p-\omega_s)t} + c.c.\end{aligned} \tag{C.4}$$

where $\mathbf{P}_p = \boldsymbol{\mu}_{fg}/V\sum_j \int d\mathbf{r} C_j e^{i[\mathbf{k_p}+j(\mathbf{k_c}-\mathbf{k_f})]\cdot\mathbf{r}}$ with $\boldsymbol{\mu}_{fg}$ being the transition dipole moment between $|g\rangle$ and $|f\rangle$ and $H_1 + H_2 = \omega_p|f_j\rangle\langle f_j| + (\omega_p - \omega_s)(|e_j\rangle\langle e_j| + |m_j\rangle\langle m_j|)$. Then, from the electromagnetic wave equation, we can obtain the following equation

$$\left(\partial_x^2 + \partial_y^2 - \frac{1}{c^2}\partial_t^2\right)\left(E_p e^{i\mathbf{k_p r}-i\omega_p t} + E_r e^{i\mathbf{k_r r}-i\omega_p t}\right) = \frac{1}{\epsilon_0 c^2}\partial_t^2 P_p e^{-i\omega_p t} \tag{C.5}$$

where $\mathbf{k_r} = \mathbf{k_p} + \mathbf{k_c} - \mathbf{k_f}$ is the wave vector of superradiance beam. Applying slowly varying envelope approximation $|(\partial_x^2 + \partial_y^2)E_{p(r)}| \ll |\mathbf{k_{p(r)}} \cdot (\partial_x E_{p(r)}\hat{\mathbf{x}} + \partial_y E_{p(r)}\hat{\mathbf{y}})|$ to Eq. (C.5), we can obtain the coupled-wave equations Eq. (8) in the main text. In the following, we will show how to solve the coupled-wave equation Eq. (8) in the main text briefly. First, starting from Eq. (8), we can obtain the following differential equation

$$\begin{aligned}&\partial_x^2 E_p + ik_0\partial_x E_p - (\beta_0^2 - ik_0\beta_0 + \kappa_{+1}\kappa_{-1})E_p = 0\\&\partial_x^2 E_r - ik_0\partial_x E_r - (\beta_0^2 - ik_0\beta_0 + \kappa_{+1}\kappa_{-1})E_r = 0\end{aligned} \tag{C.6}$$

The eigenvalues of Eq. (C.6) are $\lambda_{1,2} = -\frac{i}{2}k_0 \pm \lambda$ and $\lambda_{3,4} = \frac{i}{2}k_0 \pm \lambda$ with $\lambda = \sqrt{\beta^2 + \kappa_{+1}\kappa_{-1}}$. Then the general solution of E_p, E_r can be written as

$$\begin{aligned}E_p &= c_1 e^{\lambda_1 x} + c_2 e^{\lambda_2 x}\\E_r &= c_3 e^{(\lambda_1 + ik_0)x} + c_4 e^{(\lambda_2 + ik_0)x}\end{aligned} \tag{C.7}$$

where c_1, c_2, c_3, c_4 are indeterminate coefficients. Considering the boundary condition being $E_p(0) = E_0$, $E_r(L) = 0$ and substituting Eq. (C.7) into Eq. (C.6), we obtain the following equations to determine the coefficients c_1, c_2, c_3 and c_4 as

$$\begin{cases} c_1 + c_2 = E_0\\ c_3 e^{\lambda_1 L} + c_4 e^{\lambda_2 L} = 0\\ c_1 = \frac{i\kappa_{-1}}{\lambda_1 + \beta_0}c_3\\ c_2 = \frac{i\kappa_{-1}}{\lambda_2 + \beta_0}c_4\end{cases} \tag{C.8}$$

which give the reflectivity $R = |E_r(0)/E_p(0)|^2 = |(c_3 + c_4)/(c_1 + c_2)|^2$ as shown in Eq. (9) in the main text.

Eq. (A.4) can be expressed in the momentum space as

$$H = H_K(\mathbf{k}) + H_s(\mathbf{k}) + H_p(\mathbf{k}) \tag{C.9}$$

where $H_K = \sum_j [\mathbf{k} + \mathbf{k_p} + j(\mathbf{k_c} - \mathbf{k_f})]^2/2\,m|f_j\rangle_\mathbf{k}\langle f_j|_\mathbf{k} + [\mathbf{k} + \mathbf{k_p} - \mathbf{k_s} + j(\mathbf{k_c} - \mathbf{k_f})]^2/2\,m|e_j\rangle_\mathbf{k}\langle e_j|_\mathbf{k} + [\mathbf{k} + \mathbf{k_p} - \mathbf{k_s} + (j-1)(\mathbf{k_c} - \mathbf{k_f})]^2/2\,m|m_j\rangle_\mathbf{k}\langle m_j|_\mathbf{k}$, $H_s = \frac{1}{\Delta}\sum_j (\Omega_{c_1}^2 + \Omega_{f_1}^2)|e_j\rangle_\mathbf{k}\langle e_j|_\mathbf{k} + (\Omega_{c_2}^2 + \Omega_{f_2}^2)|m_j\rangle_\mathbf{k}\langle m_j|_\mathbf{k} + \Big[\Omega_{f_1}\Omega_{c_2}|m_j\rangle_\mathbf{k}\langle e_j|_\mathbf{k} + (\Omega_{c_1}\Omega_{c_2} + \Omega_{f_1}\Omega_{f_2})|m_{j+1}\rangle_\mathbf{k}\langle e_j|_\mathbf{k} + \Omega_{c_1}\Omega_{f_2}|m_{j+2}\rangle_\mathbf{k}\langle e_j|_\mathbf{k} + \Omega_{c_1}\Omega_{f_1}|e_{j+1}\rangle_\mathbf{k}\langle e_j|_\mathbf{k} + \Omega_{c_2}\Omega_{f_2}|m_{j+1}\rangle_\mathbf{k}\langle m_j|_\mathbf{k} + h.c.\Big]$, $H_p = \big(\sqrt{N}\Omega_p|g\rangle\langle f_0|_\mathbf{k} + \sum_j \Omega_s|e_j\rangle_\mathbf{k}\langle f_j|_\mathbf{k} + h.c.\big) - \sum_j \Delta_p|f_j\rangle_\mathbf{k}\langle f_j|_\mathbf{k} + (\Delta_p - \Delta_s)(|e_j\rangle_\mathbf{k}\langle e_j|_\mathbf{k} + |m_j\rangle_\mathbf{k}\langle m_j|_\mathbf{k})$. Then, the first two terms in Eq. (C.9) can be written in the basis of $|e_j\rangle_\mathbf{k}$ and $|m_j\rangle_\mathbf{k}$ as

Expanding the above Hamiltonian in the basis of the timed Dicke states (TDS) $|e_j\rangle_\mathbf{k} = \frac{1}{\sqrt{N}}\sum_n \exp\{i[\mathbf{k} + \mathbf{k_p} - \mathbf{k_s} + j(\mathbf{k_c} - \mathbf{k_f})]\cdot\mathbf{r_n}\}|e_n\rangle$ and $|m_j\rangle_\mathbf{k} = \frac{1}{\sqrt{N}}\sum_n \exp\{i[\mathbf{k} + \mathbf{k_p} - \mathbf{k_s} + (j-1)(\mathbf{k_c} - \mathbf{k_f})]\cdot\mathbf{r_n}\}|m_n\rangle$, with $\mathbf{k}$ being the initial momentum of atoms, Eq. (A.4) can be expressed in the momentum space and the tight-binding (TB) model is obtained.

Data availability

Data will be made available on request.

References

[1] D. Leykam, A. Andreanov, S. Flach, Adv. Phys.: X 3 (2018) 1473052.
[2] B. Sutherland, Phys. Rev. B 34 (1986) 5208.
[3] E.H. Lieb, Phys. Rev. Lett. 62 (1989) 1201.
[4] A. Mielke, J. Phys. A: Math. Gen. 24 (1991) L73.
[5] A. Mielke, J. Phys. A: Math. Gen. 24 (1991) 3311.
[6] H. Tasaki, Phys. Rev. Lett. 69 (1992) 1608.
[7] A. Mielke, Phys. Rev. Lett. 82 (1999) 4312.
[8] J. Vidal, B. Douç, R. Mosseri, P. Butaud, Phys. Rev. Lett. 85 (2000) 3906.
[9] H. Tasaki, Eur. Phys. J. B 64 (2008) 365.
[10] M.A. Springer, T.-J. Liu, A. Kuc, T. Heine, Chem. Soc. Rev. 49 (2020) 2007.
[11] Y. Cao, V. Fatemi, S. Fang, K. Watanabe, T. Taniguchi, E. Kaxiras, P. Jarillo-Herrero, Nature 556 (2018) 43.
[12] Y. Cao, V. Fatemi, A. Demir, S. Fang, S.L. Tomarken, J.Y. Luo, J.D. Sanchez-Yamagishi, K. Watanabe, T. Taniguchi, E. Kaxiras, et al., Nature 556 (2018) 80.
[13] M. Yankowitz, S. Chen, H. Polshyn, Y. Zhang, K. Watanabe, T. Taniguchi, D. Graf, A.F. Young, C.R. Dean, Science 363 (2019) 1059.
[14] J.M. Park, Y. Cao, K. Watanabe, T. Taniguchi, P. Jarillo-Herrero, Nature 590 (2021) 249.
[15] N.C. Costa, T. Mendes-Santos, T. Paiva, R.R. dos Santos, R.T. Scalettar, Phys. Rev. B 94 (2016) 155107.
[16] O. Derzhko, J. Richter, A. Honecker, M. Maksymenko, R. Moessner, Phys. Rev. B 81 (2010) 014421.
[17] C. Wu, D. Bergman, L. Balents, S.D. Sarma, Phys. Rev. Lett. 99 (2007) 070401.
[18] A. Julku, S. Peotta, T.I. Vanhala, D.-H. Kim, P. Törmä, Phys. Rev. Lett. 117 (2016) 045303.
[19] T. Löthman A. M. Black-Schaffer, Phys. Rev. B 96 (2017) 064505.
[20] E. Tang, J.-W. Mei, X.-G. Wen, Phys. Rev. Lett. 106 (2011) 236802.
[21] K. Sun, Z. Gu, H. Katsura, S.D. Sarma, Phys. Rev. Lett. 106 (2011) 236803.
[22] T. Neupert, L. Santos, C. Chamon, C. Mudry, Phys. Rev. Lett. 106 (2011) 236804.
[23] D. Sheng, Z.-C. Gu, K. Sun, L. Sheng, Nature Commun. 2 (2011) 389.
[24] F. Wang Y. Ran, Phys. Rev. B 84 (2011) 241103.
[25] D. Xiao, W. Zhu, Y. Ran, N. Nagaosa, S. Okamoto, Nature Commun. 2 (2011) 596.
[26] Y.-F. Wang, Z.-C. Gu, C.-D. Gong, D. Sheng, Phys. Rev. Lett. 107 (2011) 146803.
[27] A. Zhao S.-Q. Shen, Phys. Rev. B 85 (2012) 085209.
[28] B. Jaworowski, A. Manolescu, P. Potasz, Phys. Rev. B 92 (2015) 245119.
[29] M. Trescher E. J. Bergholtz, Phys. Rev. B 86 (2012) 241111.
[30] S. Yang, Z.-C. Gu, K. Sun, S.D. Sarma, Phys. Rev. B 86 (2012) 241112.
[31] Z. Liu, E.J. Bergholtz, H. Fan, A.M. Läuchli, Phys. Rev. Lett. 109 (2012) 186805.
[32] J.C. Budich E. Ardonne, Phys. Rev. B 88 (2013) 035139.
[33] H. Guo, S.-Q. Shen, S. Feng, Phys. Rev. B 86 (2012) 085124.
[34] D.-W. Wang, R.-B. Liu, S.-Y. Zhu, M.O. Scully, Phys. Rev. Lett. 114 (2015) 043602.
[35] L. Chen, P. Wang, Z. Meng, L. Huang, H. Cai, D.-W. Wang, S.-Y. Zhu, J. Zhang, Phys. Rev. Lett. 120 (2018) 193601.
[36] P. Wang, L. Chen, C. Mi, Z. Meng, L. Huang, K.S. Nawaz, H. Cai, D.-W. Wang, S.-Y. Zhu, J. Zhang, Npj Quantum Inf. 6 (2020) 18.
[37] C. Mi, K.S. Nawaz, L. Chen, P. Wang, H. Cai, D.-W. Wang, S.-Y. Zhu, J. Zhang, Phys. Rev. A 104 (2021) 043326.
[38] H. Cai, J. Liu, J. Wu, Y. He, S.-Y. Zhu, J.-X. Zhang, D.-W. Wang, Phys. Rev. Lett. 122 (2019) 023601.
[39] Y. He, R. Mao, H. Cai, J.-X. Zhang, Y. Li, L. Yuan, S.-Y. Zhu, D.-W. Wang, Phys. Rev. Lett. 126 (2021) 103601.
[40] R. Mao, X. Xu, J. Wang, C. Xu, G. Qian, H. Cai, S.-Y. Zhu, D.-W. Wang, Light: Sci. Appl. 11 (2022) 291.
[41] X. Xu, J. Wang, J. Dai, R. Mao, H. Cai, S.-Y. Zhu, D.-W. Wang, Phys. Rev. Lett. 129 (2022) 273603.
[42] P. Dirac, The Principles of Quantum Mechanics, Oxford University Press, 1958.
[43] W.-P. Su, J.R. Schrieffer, A.J. Heeger, Phys. Rev. Lett. 42 (1979) 1698.
[44] M. Rice E. Mele, Phys. Rev. Lett. 49 (1982) 1455.
[45] M. Creutz, Phys. Rev. Lett. 83 (1999) 2636.
[46] L. Li, C. Yang, S. Chen, Europhys. Lett. 112 (2015) 10004.
[47] C.G. Velasco B. Paredes, Phys. Rev. Lett. 119 (2017) 115301.
[48] D.-W. Wang, H. Cai, L. Yuan, S.-Y. Zhu, R.-B. Liu, Optica 2 (2015) 712.
[49] A. Shabbir S. Qamar, J. Opt. Soc. Am. B 39 (2022) 433.
[50] A. Shabbir S. Qamar, Phys. Scr. 98 (2023) 055106.